Energy, Exergy, Economic and Environmental (4E) analysis of integrated direct air capture and CO_2 methanation under uncertainty

Diederik Coppitters[a,*], Alexis Costa[b], Remi Chauvy[c,d], Lionel Dubois[e], Ward De Paepe[f], Diane Thomas[e], Guy De Weireld[b], Francesco Contino[a]

[a] *Institute of Mechanics, Materials and Civil Engineering (iMMC), Université catholique de Louvain (UCLouvain), Place du Levant, 2, 1348 Louvain-la-Neuve*
[b] *Thermodynamics and Mathematical Physics Unit, University of Mons (UMONS), Place du parc 20, 7000 Mons, Belgium*
[c] *Environmental Engineering Department, National Cheng Kung University (NCKU), Tainan City, Taiwan, Republic of China*
[d] *International Interdisciplinary Sustainability Studies Master's Degree Program, National Cheng Kung University (NCKU),Tainan City, Taiwan, Republic of China*
[e] *Chemical and Biochemical Process Engineering Unit, University of Mons (UMONS), Place du parc 20, 7000 Mons, Belgium*
[f] *Thermal Engineering and Combustion Unit, University of Mons (UMONS), Place du parc 20, 7000 Mons, Belgium*

Abstract

Direct Air Capture (DAC) technologies are gaining interest in the concept of carbon utilization and Power-to-Gas (PtG), as the economic valorization of the CO_2 into methane provides a viable pathway to allow DAC systems to mature. However, research on DAC mainly focuses on isolated systems, and the system performance depends on parameters that are highly uncertain. To study the integration of DAC in PtG, we developed a DAC-PtG model, performed an Energy, Exergy, Economic and Environmental (4E) analysis and implemented uncertainty quantification to consider the uncertain environment. The results illustrate that the DAC-PtG system is autothermal when introducing a two-

*Corresponding author
Email address: diederik.coppitters@uclouvain.be (Diederik Coppitters)

stage mechanical vapor recompression unit at the DAC outlet. The exergy efficiency ranges between 51.3% and 52.6% within 3 standard deviations, for which the uncertainty is driven by the ambient conditions and the uncertain heat of desorption. The methane issued from DAC-PtG has a lower carbon footprint than fossil methane when the carbon footprint of the electricity supply is below or equal to $0.12\,\mathrm{kg_{CO_2-eq}}$/kWh. The Levelized Cost of Synthetic Natural Gas (LCSNG) ranges between 130 €/MWh and 744 €/MWh, following an uncertain electricity price and uncertain expenses related to DAC and electrolysis. Therefore, bulk manufacturing, further maturing of these technologies and more demonstration projects are required to reduce the uncertainty of the LCSNG. Future works will consider intermittent renewable energy sources to supply power.

Keywords: 4E analysis, carbon capture and utilization, direct air capture, levelized cost of synthetic natural gas, life cycle assessment, uncertainty quantification.

---

1. Introduction

Due to the intermittent nature and location-dependent potential of solar and wind energy, these energy sources require large-scale, long-term storage and transport solutions. In addition, sector coupling is necessary to cover the overall energy demand, i.e., power-to-heat, power-to-mobility and power-to-industry. While efforts are made towards electrification of these sectors, such as heat pumps for low-grade heating [1] and electric vehicles for mobility [2],

Nomenclature

$\mathrm{CAPEX_a}$	annual capital expense, €	R_u	universal gas constant, 8.314 J/(mol K)
CE_DAC	carbon emissions induced by capturing CO_2, $\mathrm{kg_{CO_2-eq}}$	$\mathrm{SSR_{H_2O}}$	water self-sufficiency ratio
$C_\mathrm{elec,a}$	annual electricity cost, €	T	temperature, K
$\dot{E}_\mathrm{raw-SNG}$	energy flow raw SNG, W	T_cond	condensation temperature, K
F	Faraday constant, 96 485 C/mol	U_act	activation overpotential, V
GHSV	Gas Hourly Space Velocity, $\mathrm{h^{-1}}$	U_con	concentration overpotential, V
i	current density, $\mathrm{A/cm^2}$	U_oc	open-circuit potential, V
k	rate coefficient, $\mathrm{kmol}\sqrt{\mathrm{bar}}/(\mathrm{kg_{cat}\,h})$	U_ohm	ohmic overpotential, V
		U_PEM	electrolyzer potential, V
K_i	adsorption constants, $\mathrm{bar^{-1}}$	$\dot{W}_\mathrm{elec}$	electricity demand, W
LCSNG	Levelized Cost of Synthetic Natural Gas, €/MWh	$\dot{X}$	flow of total exergy, W
		$\dot{X}_\mathrm{chem}$	flow of chemical exergy, W
$\dot{m}_{\mathrm{CO_2,\ captured}}$	CO_2 captured by the system, $\mathrm{kg_{CO_2}/h}$	$\dot{X}_\mathrm{elec}$	flow of exergy of electricity demand, W
$\dot{m}_\mathrm{H_2O,DAC}$	water recovered from DAC, kg/h	$\dot{X}_\mathrm{phys}$	flow of physical exergy, W
		$\dot{X}_\mathrm{raw-SNG}$	flow of exergy raw SNG, W
$\dot{m}_\mathrm{H_2O,demand}$	water demand for electrolysis, kg/h	$\dot{X}_\mathrm{steam}$	exergy recovery in steam, W
$\dot{m}_\mathrm{H_2O,meth}$	water recovered from methanation, kg/h	$y_\mathrm{H_2O,sat}$	ratio between saturation pressure and gas pressure after compressor
$\dot{n}_\mathrm{H_2O,cond}$	amount of condensed water, mol/s	z	substance
$\dot{n}_\mathrm{H_2O,in}$	water molar flow rate entering the condenser, mol/s	Δq_{CO_2}	CO_2 working capacity, mol/kg
$\dot{n}_\mathrm{in}$	gas molar flow rate entering the condenser, mol/s	$\Delta q_\mathrm{H_2O}$	H_2O working capacity, mol/kg
$\mathrm{OPEX_a}$	annual operational expense, €	$\eta_{CO_2\ \mathrm{capture}}$	carbon capture efficiency
p	pressure, Pa	$\eta_{\dot{E}}$	energy efficiency
$p_\mathrm{H_2O,sat}$	water saturation pressure, Pa	ϕ_rh	relative humidity
$q_\mathrm{H_2O,eq}$	H_2O equilibrium loading, mol/kg	$\eta_{\dot{X}}$	exergy efficiency
$q_\mathrm{CO_2,eq}$	CO_2 equilibrium loading, mol/kg	BET	Brunauer–Emmett–Teller
$\dot{Q}_\mathrm{steam}$	heat recovery through steam, W	DAC	Direct Air Capture
R	electric resistance, Ω	PEM	Proton Exchange Membrane
r_{CH_4}	rate of reaction for CH_4, $\mathrm{kmol/(kg_{cat}h)}$	PtG	Power to Gas
		SNG	Synthetic Natural Gas

fuels remain beneficial in industries that are difficult to electrify, such as heavy-duty mobility [3], aviation [4] and high-temperature heating [5]. Such fuels

can be produced by renewable electricity (i.e., electrofuels) or biomass [6]. Essentially, electrofuels are hydrogen-based, for which the hydrogen is produced during electrolysis using renewable electricity [7]. As hydrogen in gaseous form is energy-intensive to store and transport (around $10\,\mathrm{kWh_{el}/kg_{H_2}}$ for hydrogen liquefaction [8]), hydrogen can be upgraded into other fuels with more convenient properties (e.g., Synthetic Natural Gas (SNG)). In the context of SNG, the infrastructure for natural gas liquefaction, transportation, distribution and utilisation is in place and expanding [9]. To illustrate, liquefied natural gas import terminals and export terminals are under development with a yearly capacity of 635 million tonnes of natural gas and 700 million tonnes of natural gas, respectively. Hence, converting renewable electricity into SNG (i.e., Power-to-Gas (PtG)) provides an attractive method to comply with the energy demand of existing infrastructure without additional capital costs for its distribution and use [10].

To produce renewable SNG, the methanation process requires a CO_2 feedstock [11]. The CO_2 feedstock generally originates from fossil point sources (e.g., cement production units), renewable point sources (e.g., anaerobic digestion), or the atmosphere (i.e., Direct Air Capture (DAC)) [12]. Currently, 19 DAC plants are operating worldwide, capturing around $10\,\mathrm{kt_{CO_2}/year}$ [13]. Due to the dilute CO_2 in the atmosphere (400 ppm), the energy consumption of DAC is roughly three times higher than the energy consumption of CO_2 captured from point sources [14]. However, DAC processes do not have to handle flue gas contaminants (e.g., SO_x and NO_x), it provides high geographical flexibility

and it can be used to offset CO_2 emissions from distributed sources—such as aviation—which cover roughly half of the annual CO_2 emissions [15]. Hence, DAC and CO_2 capture from point sources target different emission sources and are increasingly encouraged to be developed in parallel [16]. Fasihi et al. [17] performed a techno-economic assessment of DAC systems and estimated that DAC could become cost-competitive with point-source carbon capture in 2050, following commercialisation and massive implementation of the technology in the next decades. McQueen et al. [18] reviewed DAC technologies and highlighted the importance of learning by doing to decrease costs.

Air-captured CO_2 is gaining interest as a feedstock for PtG [19]. In this context, the economic valorization of CO_2 into SNG provides a viable pathway to allow DAC systems to further mature [20]. Veselovskaya et al. [21] proposed the adsorption of CO_2 at room temperature (using K_2CO_3/Al_2O_3 as supported sorbent), followed by the desorption and methanation between 300 °C and 350 °C (using Ru/Al_2O_3 as a catalyst) in a single circulating flow reactor. Recently, employing a dual function material in a single reactor to combine DAC and CO_2 methanation proved feasible and provided a reliable cyclic operation at isothermal operation [22] and in a temperature swing operation [23]. In a configuration with separate units, integrated solid sorbent DAC and CO_2 methanation unfold strong synergies: the waste heat from the methanation reactor can be recovered and used as a heat source during sorbent regeneration, while the co-adsorbed water can be used as feedstock for hydrogen electrolysis [24]. Water co-adsorption is generally undesired as it induces an additional

energy penalty to the CO_2 capture process. To illustrate this statement quantitatively, for a material with a CO_2:H_2O molar desorption ratio of 1:4, the heat of desorption of water ($\approx 4{\cdot}41\,\mathrm{kJ/mol_{CO_2}}$ or $630\,\mathrm{kWh/m^3_{H_2O}}$) is about twice the heat of desorption of CO_2 ($75\,\mathrm{kJ/mol_{CO_2}}$) [25]. Therefore, materials are favored with a high CO_2 selectivity over H_2O in the DAC process. In PtG in remote locations, the water supply for electrolysis mainly comes from seawater desalination [26], which is significantly less energy-demanding. More concretely, the electrical energy consumption of seawater reverse osmosis is around $3\,\mathrm{kWh/m^3}$, and the thermal energy consumption of thermal desalination processes ranges between $40\,\mathrm{kWh/m^3}$ and $80\,\mathrm{kWh/m^3}$ [27]. Nevertheless, considering desalination plants comes with an increased capital investment of the project, and these plants are expected to result in a cost of water between $0.6\,€/\mathrm{m^3}$ and $1.6\,€/\mathrm{m^3}$ in 2030 [28]. Moreover, these costs can be even higher in dry and remote regions due to higher local water demand and transportation costs, potentially limiting the geographical flexibility of PtG with DAC [17]. Therefore, as the water co-adsorption in DAC is inevitable to a certain extent, capturing and feeding it to the electrolyzer reduces the water cost and the dependency on an external water supply. Although, an external water source remains necessary to ensure a reliable water feed to the electrolyzer, as the water coming from DAC depends on the adsorption material and intermittent ambient humidity.

A 4E analysis (energy, exergy, economic and environmental) is promising to evaluate the performance of DAC-based PtG as it links the useful work with the costs and its impact on the environment [29]. In the general framework of

Carbon Capture, Utilization and Storage (CCUS), Norouzi et al. [30] studied the effects of the anolyte material used in forming formic acid by electrochemical reduction of CO_2 and water. Different scenarios were analyzed using the 4E analysis to highlight the most favourable one, linking the thermodynamic performance with cost and environmental impacts. Tian et al. [31] considered heat recovery from Liquid Natural Gas regasification in various sub-processes, including cryogenic carbon capture, and performed a 4E analysis. The results illustrated that the polygeneration system achieves high exergy efficiency (29 %), fast return on investment (7.9 years), and significant CO_2 capture (29.47 t_{CO_2}/h). In conclusion, 4E analysis provides a multi-dimensional evaluation of system performance and evaluates if a system is energy and exergy efficient, economically feasible and carbon neutral (or negative).

Novelty. Integrated DAC and CO_2 methanation systems have traditionally neglected to capitalize on the strong synergies in heat and water recovery [32], and there is a lack of comprehensive evaluation of their techno-economic and environmental performance. Besides, these technologies' techno-economic and environmental characteristics are highly uncertain, making a deterministic assessment fragile and incomplete [33]. In the framework of integrated DAC and CO_2 methanation, we provide the following three novelties: 1) exploitation of the synergies between the system components in terms of heat recovery and water recycling, 2) a comprehensive 4E analysis to assess the integration of DAC in PtG, and 3) an Uncertainty Quantification (UQ) and global sensitivity analysis to address uncertainty and validate the robustness of the results in an uncertain

operating environment. These novelties pave the way towards an optimized integration of DAC in PtG. In Section 2, the system model, the 4E analysis and the UQ method are described. Section 3 provides the energetic, exergetic, economic and environmental performance, followed by the UQ results. The paper concludes with the key messages in Section 4.

2. Method

The section starts with an overview of the model (Subsection 2.1). Thereafter, the methods for energy and water analysis (Subsection 2.2), exergy analysis (Subsection 2.3), economic analysis (Subsection 2.4) and environmental analysis (Subsection 2.5) are described. Finally, the method for UQ and global sensitivity analysis is illustrated (Subsection 2.6).

2.1. System model

The renewable methanation system with an integrated DAC unit (DAC-PtG) consists of a DAC unit, electrolyzer and methanation unit (Figure 1). The DAC unit adsorbs CO_2 and water from the ambient air. The co-adsorbed water is used as a feedstock for the electrolyzer, which converts water into hydrogen and oxygen. The CO_2 and hydrogen react in a methanation unit and form raw SNG, i.e., SNG with a methane mass fraction of around 80%. The waste heat released by this exothermic reaction (typically around 350 °C) is recovered as steam to comply with the heat demand of the DAC unit. As the primary goal of this study is to evaluate the effect of the component synergies on the overall system performance, an SNG upgrading unit for grid injection is not included.

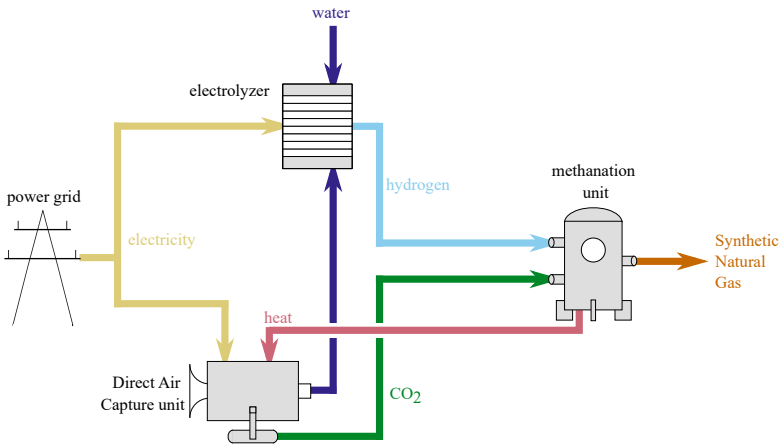

Figure 1: The simplified schematic of the power-to-gas system illustrates that the hydrogen is generated and CO_2 is captured in an electrolyzer and Direct Air Capture (DAC) unit, respectively. The hydrogen and CO_2 result in raw Synthetic Natural Gas in the methanation unit.

The system model is developed in Python. For each component, a validated model is adopted from the literature. These component models are integrated into a Python script that directs the energy, exergy and mass transfers between the components and quantifies the performance indicators. To quantify the energy, exergy and mass balances, the thermodynamic properties at each state are calculated using the Python package CoolProp [34].

2.1.1. Electrolyzer

An electrolyzer converts water into hydrogen and oxygen by using electricity:

$$2H_2O \longrightarrow 2H_2 + O_2. \tag{1}$$

Following the molar mass of the components, the water demand of electrolysis is 9 times the amount of hydrogen produced on a mass basis, i.e., $\dot{m}_{H_2O,electrolysis} =$

$9\dot{m}_{\mathrm{H_2}}$. The main, mature electrolyzer technologies are alkaline electrolysis and Polymer Electrolyte Membrane (PEM) electrolysis. While alkaline electrolysis is the most mature and cheapest technology (800 €/kW - 1500 €/kW), it suffers from low current densities (0.25 A/cm^2 - 0.45 A/cm^2) and a constrained operating range (20 % - 100 %). Instead, PEM electrolyzers offer a full load range, compactness (i.e., high current densities up to 2 A/cm^2) and fast response time, at the expense of higher costs (1400 €/kW - 2100 €/kW) [35]. We adopted a PEM electrolyzer technology, as its characteristics provide significant benefits when coupled with an intermittent energy supply [36].

To model the electrolyzer behaviour and corresponding energy consumption, we adopted and integrated the model from Abdin et al. [37], which has been validated with experimental current-voltage curves from Marangio et al. [38]. The model quantifies the voltage-current relation as follows:

$$U_{\mathrm{PEM}} = U_{\mathrm{oc}} - U_{\mathrm{act}} - U_{\mathrm{ohm}} - U_{\mathrm{con}}. \tag{2}$$

The open-circuit voltage U_{oc} is derived from the Nernst equation for water electrolysis. To transfer the electrons between the electrodes, an overpotential has to be applied, i.e., the activation overpotential U_{act}. The concentration overpotential U_{con} occurs at high current densities and is created due to an excess of reactants (e.g., oxygen bubbles slowing down the reaction). Finally, the ohmic overpotential U_{ohm} overcomes the electric resistance of the electrodes, bipolar plates and the membrane. We refer to Abdin et al. [37] for the details on quantifying these overpotentials.

Following the voltage-current relation, the operating current of the electrolyzer can be defined, based on the applied power. From this operating current I, the hydrogen molar flow rate $\dot{n}_{\mathrm{H_2}}$ can be quantified:

$$\dot{n}_{\mathrm{H_2}} = \frac{I}{2F}. \tag{3}$$

As the electrolyzer works over the thermoneutral voltage (U_{tn}), excess heat will be generated. The excess heat corresponds to [39]:

$$\dot{Q}_{\mathrm{PEM}} = (U_{\mathrm{PEM}} - U_{\mathrm{tn}})\, I, \tag{4}$$

where the thermoneutral voltage represents the voltage covering the energy of the water-splitting reaction [40].

2.1.2. Direct air capture unit

Roughly, DAC is classified into two categories: using either liquid sorbents or solid sorbents [41]. For DAC using a liquid sorbent, the regeneration and calcination of the sorbent occurs at high temperature (900 °C) [42], the regeneration step for DAC using a solid sorbent is performed at low temperature (100 °C). We adopted a solid sorbent DAC technology, as the low operating temperature (100 °C) allows waste heat recovery from the methanation unit (operating at 350 °C). Moreover, it co-adsorbs water, which can be recycled to feed the electrolysis [25]. The adsorption is performed on an amine grafted ion exchanger resin (Lewatit VP OC 1065), for which Veneman [43] performed an experimental characterization of the adsorption isotherms. These adsorption

isotherms are integrated in the equilibrium based adsorption-desorption process model from Drechsler et al. [25].

In the model, the CO_2 equilibrium loading $\left(q_{CO_{2,eq}}\right)$ follows a Toth model:

$$q_{CO_{2,eq}} = \frac{q_{max,Toth}\ b_{Toth}\ p_{CO_2}}{\left(1 + (b_{Toth}\ p_{CO_2})^{t_{Toth}}\right)^{\frac{1}{t_{Toth}}}}, \tag{5}$$

where the equations for the Toth isotherm parameters (b_{Toth}, $q_{max,Toth}$ and t_{Toth}) are developed in Drechsler et al. [25], based on experiments from Veneman [43]. The co-adsorption of water on Lewatit can be approximated by a Brunauer–Emmett–Teller (BET) model:

$$\frac{q_{H_2O,eq}}{q_{H_2O,eq,mono}} = \frac{c_{BET}\ \phi_{rh}}{1-\phi_{rh}} \frac{1 - (n_{BET}+1)\,\phi_{rh}^{n_{BET}} + n_{BET}\ \phi_{rh}^{n_{BET}+1}}{1 + (c_{BET}-1)\,\phi_{rh} - c_{BET}\ \phi_{rh}^{n_{BET}+1}}, \tag{6}$$

where a monolayer loading ($q_{H_2O,eq,mono}$) of 2.933 mol/kg, the number of layers (n_{BET}) being 7.680 and an affinity (c_{BET}) of 6.257 are matched on experimental values [25]. Equation 6 illustrates that the equilibrium loading of water on Lewatit can be expressed in terms of the relative humidity (ϕ_{rh}). Considering a counter-current, isothermal sorbent regeneration unit, the working capacities (Δq_{CO_2} and Δq_{H_2O}) are formulated with respect to the CO_2 and water loading at the regeneration outlet ($q_{CO_2,work}$ and $q_{H_2O,work}$, respectively) [25]:

$$q_{\mathrm{CO_2,work}} = q_{\mathrm{CO_2,eq,amb}} - \Delta q_{\mathrm{CO_2}}, \tag{7}$$

$$q_{\mathrm{H_2O,work}} = q_{\mathrm{H_2O,eq,amb}} - \Delta q_{\mathrm{H_2O}}, \tag{8}$$

where $q_{\mathrm{CO_2,eq,amb}}$ and $q_{\mathrm{H_2O,eq,amb}}$ correspond to the CO_2 and water loading under ambient conditions, respectively. Following the assumption of equilibrium of the gas and solid phase in the adsorber, the relation between both working capacities depends on the working pressures:

$$\frac{p_{\mathrm{CO_2,work}}}{\Delta q_{\mathrm{CO_2}}} = \frac{p_{\mathrm{H_2O,work}}}{\Delta q_{\mathrm{H_2O}}}, \tag{9}$$

where the working pressures depend on the desorption temperature and the equilibrium loading under ambient conditions. Additional details on the equilibrium adsorber unit are provided in Drechsler et al. [25]. The relation between both working capacities illustrates that increasing the desorption temperature reduces the water co-desorption down to a molar ratio H_2O:CO_2 of 4:1 at a desorption temperature of 100 °C (Figure 2), i.e., $\dot{m}_{\mathrm{H_2O,DAC}} = 4\frac{M_{\mathrm{H_2O}}}{M_{\mathrm{CO_2}}}\dot{m}_{\mathrm{CO_2}}$.

The heat of desorption of CO_2 and H_2O and the heat capacity of the sorbent are estimated at $\Delta H_{\mathrm{des,CO_2}} = 75\,\mathrm{kJ/mol}$ [44], $\Delta H_{\mathrm{des,H_2O}} = 43\,\mathrm{kJ/mol}$ [44] and $c_{\mathrm{sorbent}} = 1.5\,\mathrm{kJ/kgK}$ [43]. At a desorption temperature of 100 °C and a H_2O:CO_2 molar ratio of 4:1, the thermal energy requirement corresponds to 385 kJ per mole of CO_2 captured. Thus, the co-adsorption of water in the DAC unit results in a significant energy penalty. Note that for DAC systems,

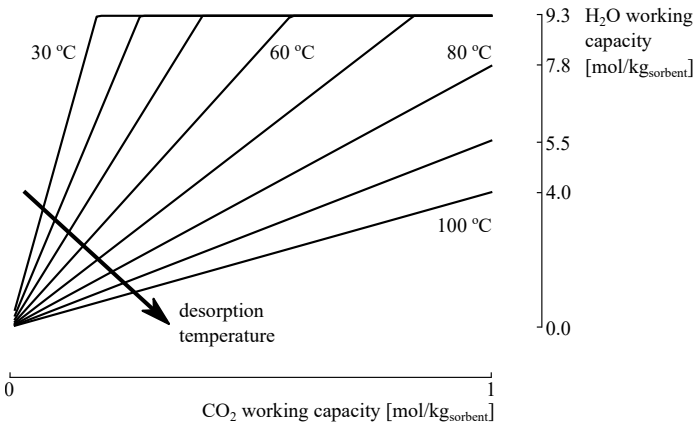

Figure 2: The working capacity of H_2O with respect to the working capacity of CO_2 for different desorption temperatures illustrates that the co-adsorption of H_2O reduces with the increase of desorption temperature. The isotherms used are at ambient air temperature of 25 °C and 80% relative humidity, at desorption temperature from 30 °C to 100 °C, in steps of 10 °C.

pre-drying of the feed gas (ambient air) to remove the water is considered unaffordable due to the large amount of ambient air required per unit of CO_2 captured (ratio of air to CO_2 molecules equals 2500:1) [45]. The thermal energy demand of the DAC unit is highly dependent on the ambient temperature and relative humidity. Therefore, the heat release during methanation might not be consistently sufficient over the entire lifetime of the DAC-PtG system. Thus, an additional heat source is required to ensure a reliable operation.

2.1.3. Mechanical vapor recompression

To recuperate the heat of desorption of H_2O spent during the DAC process, we integrated a Mechanical Vapor Recompression (MVR) unit. Connecting an MVR unit to the DAC outlet stream was recently introduced by Drechsler et al. [24, 25, 32] to recuperate the heat from the desorbed water vapor. Briefly, in an MVR unit, the gas is compressed and cooled consecutively

to recuperate the latent heat from the vapor and remove the condensed water. Although the process introduces additional electricity demand (and thus high-value exergy), the resulting pressurized DAC product stream results in higher equilibrium conversion and faster kinetics during methanation (see Subsection 2.1.4) [24]. In other words, the additional power demand to pressurize the DAC product stream can be relativized, as it results in pressurized CO_2 at the inlet of the methanation unit.

The vapor compressor is modelled assuming an ideal gas mixture and an isentropic efficiency of 70 % [25]. After the vapor compressor, the gas is sent to a condenser, which operates at a temperature difference of 10 °C with the desorption process, to ensure a minimal heat transfer driving force (i.e., $T_{\mathrm{cond}} = T_{\mathrm{des}}+10\,^{\circ}\mathrm{C}$). Assuming a phase equilibrium at the condenser outlet, i.e., $p_{\mathrm{H_2O}} = p_{\mathrm{H_2O,sat}}(T_{\mathrm{cond}})$, no pressure losses and no heat losses, the amount of condensed water ($\dot{n}_{\mathrm{H_2O,cond}}$) corresponds to [25]:

$$\dot{n}_{\mathrm{H_2O,cond}} = \frac{\dot{n}_{\mathrm{H_2O,in}} - \dot{n}_{\mathrm{in}}\ y_{\mathrm{H_2O,sat}}}{1 - y_{\mathrm{H_2O,sat}}}, \tag{10}$$

where $\dot{n}_{\mathrm{H_2O,in}}$, $\dot{n}_{\mathrm{in}}$ and $y_{\mathrm{H_2O,sat}}$ correspond to the amount of water entering the condenser, the amount of gas entering the condenser and the ratio between the water saturation pressure and the gas pressure after the compressor.

2.1.4. Methanation unit

We adopted a most popular catalytic methanation method to convert the CO_2 and H_2 into SNG [46]. The methanation unit consists of a typical four

series-connected adiabatic fixed bed reactors, to reach a sufficient CO_2 conversion into CH_4, based on the design described by Chauvy et al. [47]. The design includes intermediate cooling steps, to control the reaction temperature and thus to avoid coking and sintering of the catalyst [48]. A Ni-based catalyst ($Ni/MgAl_2O_4$, Ni 15 wt%) and a reaction temperature of 350 °C is considered [47]. In the reactor, the Sabatier reaction occurs:

$$CO_2 + 4H_2 \rightleftharpoons CH_4 + 2H_2O \qquad \Delta H_{298} = -165 \text{ kJ/mol}. \tag{11}$$

As the reaction is exothermic, the product stream increases in temperature. However, up to 650 °C and at 10 bar, mainly the species involved in the Sabatier reaction are present in the outlet stream [48]. In addition, the stoichiometric ratio (H_2:CO_2 = 4) is selected, as it results in a complete conversion of CO_2 [48]. Therefore, only the Sabatier reaction is considered during methanation. The reaction rate of CH_4 (r_{CH_4} in kmol/(kg_{cat}h)) is obtained by the Langmuir–Hinshelwood–Hougen–Watson approach [48]:

$$r_{CH_4} = -\frac{k}{p_{H_2}^{3.5}} \frac{p_{CH_4}\, p_{H_2O}^2 - \frac{p_{H_2}^4\, p_{CO_2}}{K}}{\left(1 + K_{CO} p_{CO} + K_{H_2} p_{H_2} + K_{CH_4} p_{CH_4} + \frac{K_{H_2O} p_{H_2O}}{p_{H_2}}\right)^2}, \tag{12}$$

where p_i corresponds to the partial pressures of the different components in the reaction ($i \in \{CH_4, CO_2, H_2O, H_2, CO\}$), k is the rate coefficient depending on the reaction temperature and K_i are the adsorption constants for the reaction

components. The Gas Hourly Space Velocity (GHSV) in each reactor is maintained close to 4000 h^{-1} [47]. We refer to Chauvy et al. [47] for additional details on the design of the methanation unit and the quantification of the parameters in the reaction rate equation.

Heat exchangers bring the gas inlet stream temperature back to 350 °C at each reactor. We assumed an ideal heat exchanger without heat losses to the environment [24]. To reduce the outlet temperature from the first reactor and preheat the incoming H_2 and CO_2 streams, 70 % of the gas at the outlet of the first reactor is recycled [48]. Finally, the outlet gas stream is cooled down after the fourth reactor, and the remaining water is extracted. Ideally, 2 moles of water are extracted per mole of CH_4 produced, resulting in a water flow rate as a by-product of methanation ($\dot{m}_{H_2O,meth}$).

2.2. Energy and water analysis

The energy efficiency ($\eta_{\dot{E}}$) of the DAC-PtG system is defined as:

$$\eta_{\dot{E}} = \frac{\dot{E}_{raw-SNG} + \dot{Q}_{steam}}{\dot{W}_{elec}}, \tag{13}$$

where $\dot{E}_{raw-SNG}$ is the energy flow of the produced raw SNG on an LHV-basis, considering both methane and hydrogen contributing to the energy density. $\dot{Q}_{steam}$ is the remaining waste heat (if any) from the methanation unit in the form of steam, after complying with the heat demand of the DAC unit, and $\dot{W}_{elec}$ is the amount of electricity provided to the system.

The water self-sufficiency ratio (SSR_{H_2O}) indicates self-sufficiency in terms

of water supply. In other words, the quantity indicates the amount of water recycled within the DAC-PtG system. While the system requires water for electrolysis ($\dot{m}_{\mathrm{H_2O,electrolysis}}$, defined in Subsection 2.1.1), water can be recovered from the DAC ($\dot{m}_{\mathrm{H_2O,DAC}}$, defined in Subsection 2.1.2) and methanation unit ($\dot{m}_{\mathrm{H_2O,meth}}$, defined in Subsection 2.1.4):

$$\mathrm{SSR}_{\mathrm{H_2O}} = \frac{\dot{m}_{\mathrm{H_2O,DAC}} + \dot{m}_{\mathrm{H_2O,meth}}}{\dot{m}_{\mathrm{H_2O,electrolysis}}}. \tag{14}$$

Note that the water in the cooling circuit for the methanation unit is not considered in the self-sufficiency ratio, as it is assumed that the cooling water is recuperated once it released its energy in a subsequent process, e.g., a steam turbine.

2.3. Exergy analysis

An exergy analysis is adopted as the energy streams for the DAC-PtG system are defined by different qualities (i.e., power, heat and SNG). Neglecting the kinetic and potential exergy, the flow of total exergy ($\dot{X}$) represents the combined thermophysical and chemical exergy flows [49]:

$$\dot{X} = \dot{X}_{\mathrm{phys}} + \dot{X}_{\mathrm{chem}}. \tag{15}$$

The thermophysical exergy corresponds to the obtainable work when the flow is brought from its process state (T, p, z) to the environmental state (T_0, p_0, z). The chemical exergy is the obtainable work when the flow is brought from the environmental state to the standard dead state (T_0, p_0, z_0) [49]. The exergy rate

of heat input is quantified by [49]:

$$\dot{X}_{\text{heat}} = \dot{Q}\left(1 - \frac{T_0}{T}\right) \tag{16}$$

We assume Standard Ambient Temperature and Pressure [50] (25 °C, 1 bar and 80% relative humidity) as the standard dead state.

With the total exergy, the exergy efficiency of the system is quantified. The exergy efficiency ($\eta_{\dot{X}}$) corresponds to the amount of exergy available at the system output, in the form of raw SNG ($\dot{X}_{\text{raw-SNG}}$) and steam ($\dot{X}_{\text{steam}}$), per unit of exergy supplied, i.e., the power provided to the components ($\dot{X}_{\text{elec}}$):

$$\eta_{\dot{X}} = \frac{\dot{X}_{\text{raw-SNG}} + \dot{X}_{\text{steam}}}{\dot{X}_{\text{elec}}}. \tag{17}$$

2.4. Economic analysis

The Levelized Cost of Synthetic Natural Gas (LCSNG) indicates the system cost per unit of energy in the raw SNG:

$$\text{LCSNG} = \frac{\text{CAPEX}_{\text{a}} + \text{OPEX}_{\text{a}} + C_{\text{elec,a}}}{E_{\text{raw-SNG}}}, \tag{18}$$

where $E_{\text{raw-SNG}}$ corresponds to the annualized energy content of the SNG, considering both methane and hydrogen contributing to the SNG. The energy content of SNG is on an LHV-basis, assuming that the heat of vaporization of water is not recuperated, i.e., the conservative scenario. CAPEX_{a}, OPEX_{a} and $C_{\text{elec,a}}$ correspond to the annualized capital expenses, operating expenses and the annualized cost of electricity, respectively. Additional details on the

quantification of these parameters is described by Zakeri et al. [51]. The initial assumptions on the economic parameters for the components and the entire system are listed in Table 1 and Table 2, respectively.

Table 1: The cost parameters used for the components.

component	CAPEX	OPEX	Ref.
electrolyzer	1750 €/kW	4 % of CAPEX	[36]
direct air capture	730 €/t_{CO_2}/year	4 % of CAPEX	[17]
methanation	735 €/kW_{SNG}	29 €/kW_{SNG}/year	[26]
compressor	1000 €/kW	2 % of CAPEX	[52]

Table 2: The cost parameters used for the entire system.

parameter	value	Ref.
electricity price	40 €/MWh	[47]
inflation rate	2 %	[53]
interest rate	6 %	[47]
indirect capital costs ratio	1.44	[47]

2.5. Environmental analysis

In the environmental analysis, the GHG emissions of CO_2 captured from DAC to produce raw SNG are quantified, using 1 MJ of raw SNG (LHV) as a functional unit. The GHG emissions from the materials needed for the infrastructure of the different facilities and GHG emissions from the material, water and energy use during operations are included. We compile the necessary inventory data for the DAC-PtG system from different sources. The inventory for the DAC infrastructure is adopted from Deutz and Bardow [54] and Madhu et al. [55]. The infrastructure of the methanation unit is based on the description provided by Chauvy et al. [47, 56], while aggregated data are considered for the PEM electrolyzer based on the detailed inventory from

Bareiß et al. [57]. We evaluate the inputs of chemicals, water, and energy required during the operation of the DAC-PtG system. Inventory data related to the necessary materials are gathered from Deutz and Bardow [54], Madhu et al. [55], and Chauvy et al. [56]. We do not consider an environmental credit for byproducts, such as O_2 generated during H_2 production.

To determine the performance of the DAC system, a carbon capture efficiency metric ($\eta_{\mathrm{CO_2\ capture}}$) is adopted [54]:

$$\eta_{\mathrm{CO_2\ capture}} = \frac{\dot{m}_{\mathrm{CO_2,\ captured}} - CE_{\mathrm{DAC}}}{\dot{m}_{\mathrm{CO_2,\ captured}}}, \tag{19}$$

where CE_{DAC} is the total amount of carbon emissions induced by capturing CO_2. A positive carbon capture efficiency ($\eta_{\mathrm{CO_2\ capture}} > 0$) implies that more CO_2 is captured than emitted by the DAC system, while a negative carbon capture efficiency ($\eta_{\mathrm{CO_2\ capture}} < 0$) indicates that more CO_2 is emitted than captured. We include two environmental metrics, i.e., the Climate Change (CC) and Fossil Depletion (FD) impacts, as they reflect the main motivation for deploying a DAC-PtG system. All processes are considered on-site, neglecting the environmental impacts and transport and storage energy requirements.

2.6. Uncertainty quantification and global sensitivity analysis

The quantities of interest to determine the performance of the system in an energy, exergy, economic and environmental aspect are highly uncertain and likely to vary during the operation of the system. Among others, the weather parameters (ambient temperature and humidity) are intermittent, the actual

CAPEX and OPEX are subject to an active evolving and maturing of the technologies, the timespan between feasibility study and investment and unexpected operating costs [58]. Therefore, we conducted a UQ and global sensitivity analysis to quantify the uncertainty on the quantities of interest and to identify the dominating parameter uncertainties. The uncertainty ranges on the parameters are provided in Table 3.

Table 3: The ranges considered on the uncertain parameters for uncertainty quantification and global sensitivity analysis.

parameter	min	max	unit	Ref.
c_{elec}	40	250	€/MWh	[47, 59]
inflation rate	1	3	%	[53]
interest rate	4	8	%	[47]
$\text{CAPEX}_{\text{PEM}}$	1400	2100	€/kW	[36]
OPEX_{PEM}	3	5	%	[36]
$\text{CAPEX}_{\text{DAC}}$	250	1220	€/t_{CO_2}/year	[17]
OPEX_{DAC}	2	6	%	[36]
$\text{CAPEX}_{\text{meth}}$	450	1020	€/kW	[47, 60, 61]
$\text{OPEX}_{\text{meth}}$	20	40	€/kW	[47, 60]
$\text{CAPEX}_{\text{compr}}$	1000	1500	€/kW	[3]
$\text{OPEX}_{\text{compr}}$	1	2	%	[3]
$\Delta H_{\text{des},H_2O}$	40	45	kJ/mol	[44]
$\Delta H_{\text{des},CO_2}$	70	80	kJ/mol	[44]
T_{amb}	5	25	°C	
RH	40	100	%	

To perform UQ and global sensitivity analysis in a computationally-efficient way, we adopted Polynomial Chaos Expansion (PCE). This surrogate-assisted UQ technique allows deriving the distribution parameters and the sensitivity indices (i.e., Sobol' indices) analytically from the coefficients that characterize the surrogate model [35]. To apply PCE on the DAC-PtG system, we used the open-source Python framework RHEIA [62], co-developed by the lead author of this paper. We adopted a polynomial order of 2 and—according to the conventional

truncation scheme—generated 272 training samples to result in a Leave-One-Out error below 1 % for each quantity of interest of the DAC-PtG system [63]. Once the PCE is constructed, the statistical moments and sensitivity indices (i.e., Sobol' indices) can be derived from the PCE coefficients analytically, i.e., no more model evaluations are required. We refer to Sudret et al. [63] for a comprehensive overview of the PCE method.

3. Results and discussion

First, the power, heat and mass exchange between the different components is evaluated and the energy efficiency is quantified (Subsection 3.1). The 4E analysis is completed with the exergy analysis (Subsection 3.2), economic analysis (Subsection 3.3) and environmental analysis (Subsection 3.4). The section concludes with the UQ and global sensitivity analysis, to evaluate the robustness of the results (Subsection 3.5).

3.1. Energy and water analysis

To illustrate the operating conditions of the proposed DAC-PtG system, a flow sheet is presented in Figure 3. The size of the system is based on the validated PtG system in Chauvy et al. [47]. The size of the DAC unit is roughly double the size of existing commercial solid sorbent DAC units (up to 4000 t_{CO_2}/year), but fits in the scale of projected DAC units [64]. Air enters the DAC unit based on the Standard Ambient Temperature and Pressure [50], namely 25 °C, 1 atm and $\phi_{rh} = 80\,\%$, with the help of fans (0.24 MW_e). In the adsorber, CO_2 and water are adsorbed at ambient conditions. When saturated,

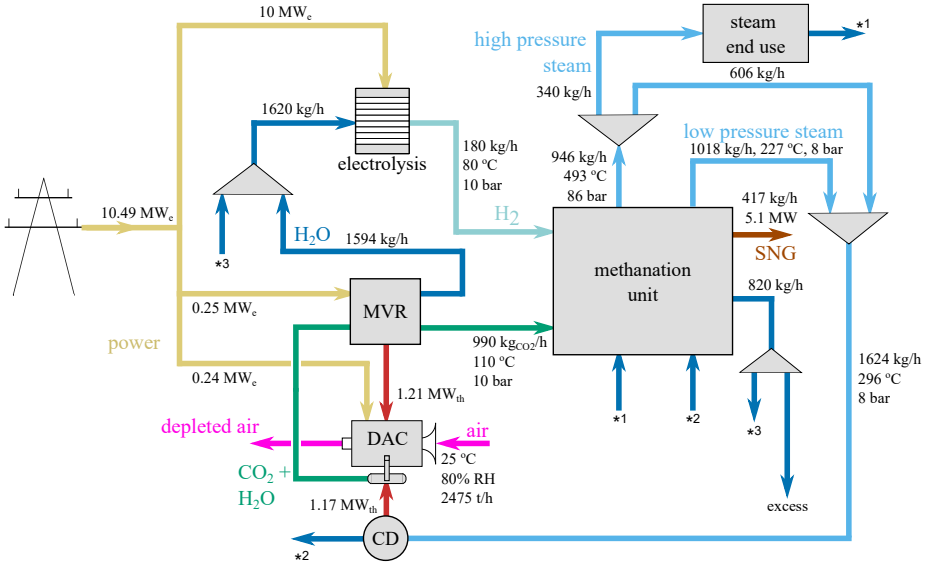

Figure 3: The hydrogen is produced by electrolysis, while the CO_2 is captured by Direct Air Capture (DAC), followed by compression in a Mechanical Vapor Recompression (MVR) unit. Both products produce Synthetic Natural Gas (SNG) in a methanation unit. The excess heat during methanation is recuperated in high-pressure and low-pressure steam, which is partly used to provide the remaining heat demand for the DAC through a condenser (CD).

the sorbent is regenerated at a desorption temperature of 100 °C, which results in a gas outlet stream containing 990 kg_{CO_2}/h and 1661 kg_{H_2O}/h. This corresponds to a H_2O:CO_2 molar adsorption ratio of 4:1. The regeneration process requires 2.38 MW_{th} to heat the sorbent and to desorb the H_2O and CO_2.

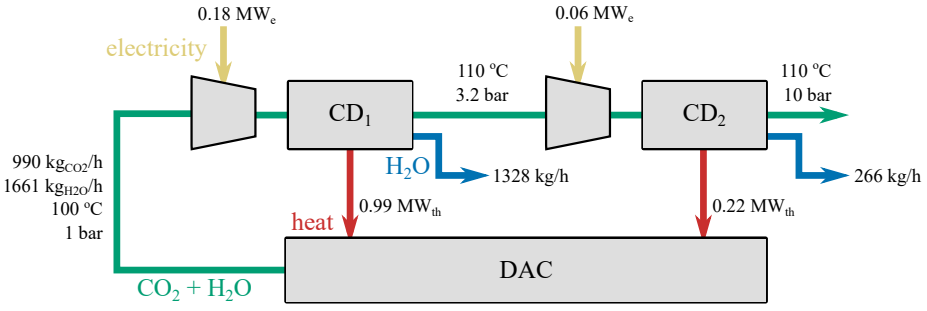

Figure 4: A two-stage mechanical vapor recompression is considered. In each stage, the product stream is compressed and cooled in a compressor and condenser (CD). Following the condensation, heat is recovered and supplied to the Direct Air Capture (DAC) unit.

After the DAC unit, an MVR unit is installed, characterized by a two-stage compressor-condenser unit (Figure 4). In the first stage, the stream is compressed to 3.2 bar and the thermal energy of the stream is largely recovered ($0.99\,\mathrm{MW_{th}}$) in the condenser. As the condenser outlet temperature remains 10 °C above the DAC desorption temperature (i.e., 110 °C), the recovered heat can be used as a heat source for the DAC unit. In addition, $1328\,\mathrm{kg_{H_2O}/h}$ of water is removed from the gas stream. In the second stage, a similar process is performed: the remaining CO_2-H_2O mixture is compressed up to 10 bar, whereafter it is cooled down in the condenser, supplying $0.22\,\mathrm{MW_{th}}$ to the DAC unit and removing an additional $266\,\mathrm{kg_{H_2O}/h}$ of water from the gas stream. The heat recovery process in MVR requires $0.25\,\mathrm{MW_e}$ to realize the compression of the product stream up to 10 bar.

Hydrogen is produced in a pressurized PEM electrolyser unit. To produce $180\,\mathrm{kg_{H_2}/h}$, the electrolyzer consumes $10.0\,\mathrm{MW_e}$ and $1620\,\mathrm{kg_{H_2O}/h}$. The PEM electrolyser unit is the main power-consuming unit in the DAC-PtG system (95% of the total power demand is due to electrolysis). The hydrogen is considered pure and enters the methanation unit at 80 °C and 10 bar.

The methanation unit produces raw SNG in four consecutive reactors (Figure 5). In the first reactor, a high mass flow rate (4124 kg/h) reacts, whereafter 70 % (2887 kg/h) is recycled to preheat the inlet stream. The four reactors subsequently increase the content of CH_4 and H_2O in the product stream (Table 4). In each consecutive reactor, fewer reactants are available, which results in a consecutive reduction in gain in CH_4 mass fraction. Consequently, the temperature

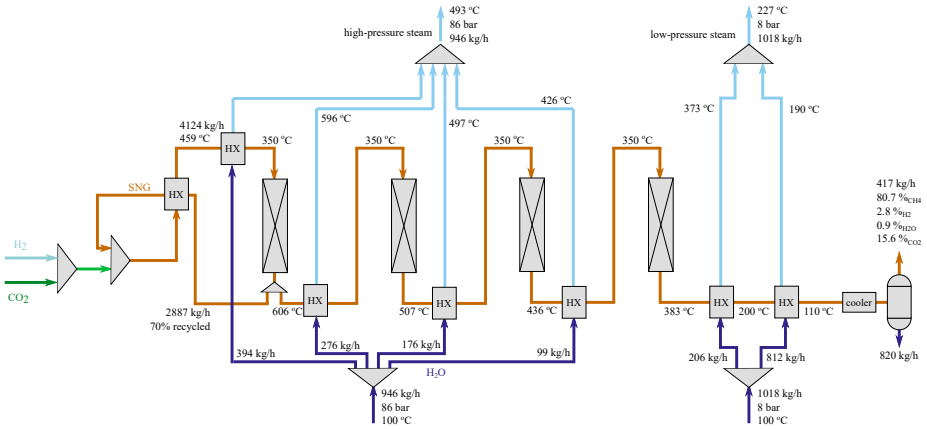

Figure 5: The methanation unit consists of four subsequent reactors. In between each reactor, the reactant is cooled using high-pressure water in heat exchangers (HX). After the final reactor, the remaining reactant is cooled using low-pressure steam, followed by a flash unit to remove the water content in the produced Synthetic Natural Gas (SNG).

Table 4: The mass fractions of the components in the product stream after each reactor.

	mass fraction [%]			
	CH_4	H_2O	H_2	CO_2
reactor 1	20.9	52.4	4.1	22.6
reactor 2	24.5	60.6	2.3	12.6
reactor 3	26.5	64.9	1.3	7.3
reactor 4	27.2	66.6	0.9	5.3
after cooling	80.7	0.9	2.8	15.6

of the product stream after each reactor reduces: 606 °C after the first reactor, 507 °C after the second reactor, 436 °C after the third reactor and 383 °C after the fourth reactor. As the product mass flow rate remains the same, the amount of coolant water after each reactor is reduced proportionally with the decrease in product temperature to ensure that the product stream enters the next reactor at 350 °C.

To improve the energy recovery in each heat exchanger (HX), the cooling water is pressurized (86 bar). In addition, a pinch analysis is performed to ensure that the cooling water leaves the heat exchanger in the form of steam

411 at 10 °C below the hot stream inlet temperature (i.e., the temperature of the
412 product stream leaving each reactor). Combined, the steam produced in the
413 first four HXs results in 946 kg/h of steam at 86 bar and 493 °C. In the fifth
414 and sixth HX, the product gas is cooled down to recuperate the sensible heat
415 of the gas and the latent heat from the water vapor. In addition, the liquid
416 water is removed from the product stream, resulting in a significant increase in
417 the share of CH_4 in the raw SNG (from 27.2 % to 80.7 %, Table 4). The HXs
418 are designed such that the cooling water leaves the HXs at 10 °C below the
419 hot stream inlet temperature. In this case, the water pressure is lower (8 bar),
420 following the lower outlet temperature of the product stream. Combined, the
421 fifth and sixth HX generate 1018 kg/h of steam at 8 bar and 227 °C.

422 The produced steam is recycled in the system to comply with the remaining
423 heat demand in the DAC unit (Figure 3). In total, 1624 kg_{H_2O}/h (83% of
424 the total amount) is condensed to provide the remaining heat for the DAC
425 unit (1.17 MW_{th}). The remaining high-pressure steam can be used for other
426 purposes outside the DAC-PtG system. The excess steam can be used in various
427 applications, such as food, paper, chemical and plastics processing [65]. We
428 assume that the steam returns to the methanation unit, in the form of liquid
429 cooling water at 100 °C and 1 bar, whereafter it is compressed up to the required
430 pressure by pumps. As the electricity demand of the pumps (7 kW) is several
431 orders of magnitude smaller than the other components, the pumps are not
432 presented on the system overview.

433 In conclusion, 417 kg_{SNG}/h is produced, containing 80.7 $\%_{mass}$ CH_4 and

2.8 $\%_{mass}$ H_2. Following the heat recovery in the methanation unit and the MVR unit, the system operates autothermally. In addition, considering the water recovery in the MVR unit (1594 kg/h) and the methanation unit (820 kg/h), the system does not depend on an external water supply to comply with the water demand for electrolysis (1620 kg/h). Note that this calculation assumes a fixed ambient environment, and any variations in ambient conditions may result in changes to the water recovery. Finally, with a total power demand of 10.49 MW_e, a power content available in the SNG stream of 5.06 MW (LHV-basis) and excess steam of 0.28 MW (i.e., enthalpy difference between water inlet and outlet of the methanation unit, minus the heat for the DAC unit), the system reaches an energy efficiency of 51.1 %.

3.2. Exergy analysis

A Grassmann diagram evaluates the exergy destruction in each component of the DAC-PtG system (Figure 6).

Electrolysis results in the highest exergy destruction (3.96 MW). These irreversibilities are induced by the overpotential applied to the electrolyzer to realize the electron transfer. The DAC unit with MVR results in an exergy destruction of 0.94 MW, due to preheating of the sorbent and condensation in the MVR. Nevertheless, the exergy destruction in the DAC unit with MVR is limited (19 %) when compared to the overall exergy destruction in the DAC-PtG system (5.04 MW). The produced raw SNG carries an exergy content of 5.28 MW, while the excess high-pressure steam carries 0.18 MW. 0.10 MW of exergy is destroyed in the heat exchangers in the methanation unit. Combining

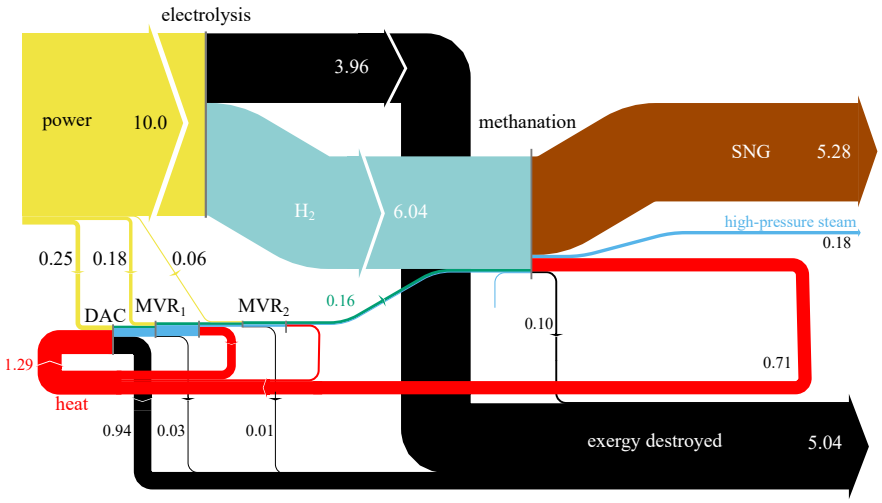

Figure 6: The Grassmann diagram (values in MW) illustrates that the major exergy destruction occurs during electrolysis. The remaining exergy destruction occurs in the Direct Air Capture (DAC) unit.

the exergy in the raw SNG (5.28 MW) and steam (0.18 MW), the DAC-PtG system reaches an exergy efficiency of 52.2 %.

Due to the overpotentials in the PEM electrolyser, a significant amount of heat is released into the environment (1.52 MW_{th}). Considering that the waste heat has a temperature of 80 °C, the cooling water to recover that heat can be heated up to 75 °C [66]. As the water temperature is rather low, the amount of exergy recovered from PEM electrolysis is small (0.22 MW). Consequently, introducing PEM waste heat recovery improves the exergy efficiency of the DAC-PtG system by only 2 $\%_{abs}$. Nevertheless, the low-grade heat can be supplied to, e.g., district heating networks, which typically operate near 75 °C [66].

3.3. Economic analysis

To evaluate the economic feasibility, the LCSNG is quantified. Considering the initial assumptions on the economic parameters (Table 1 and Table 2), the LCSNG corresponds to 180 €/MWh. This value situates near existing values present in the literature: Chauvy et al. [47] performed a techno-economic study on a renewable methanation plant, considering CO_2 capture from a cement plant, and presented a value of 170 €/MWh for raw SNG with similar quality than the raw SNG achieved by the DAC-PtG system. They considered the same price for electricity as in this study. However, these results are sensitive to the deterministic assumptions on the techno-economic parameters. In Subsection 3.5, a UQ and global sensitivity analysis is performed to quantify the importance of the uncertain parameters on the LCSNG.

The cost breakdown illustrates that the main cost is related to hydrogen production (79 %, Figure 7). Due to the high power demand for electrolysis, nearly half of that cost (45 %) relates to buying electricity to produce hydrogen. In contrast, 34 % corresponds to the PEM electrolyzer equipment cost, i.e., indirect cost, investment cost and operating and maintenance cost. The DAC unit cost is noticeable (13 %), and the expenses related to the DAC unit during investment are 23 % of the total investment cost of the DAC-PtG system. In conclusion, as the total cost is dominated by the cost related to electrolysis, the choice of technology to provide the CO_2 for methanation has a limited effect on the cost of producing SNG.

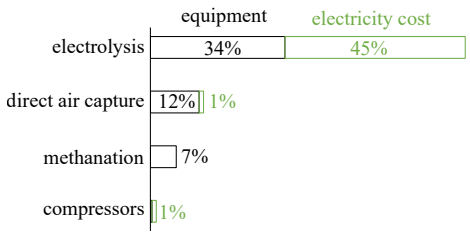

Figure 7: Breaking down the costs illustrates that the electrolyzer is the dominant component. The equipment cost corresponds to the CAPEX + OPEX, while the electricity cost corresponds to the cost for electricity to run the unit.

3.4. Environmental analysis

The environmental performance of the DAC-PtG system depends significantly on the power source (Table 5). When the power is produced by a renewable energy source, i.e., wind ($0.011\,\mathrm{kg_{CO_2-eq}/kWh}$) and solar ($0.044\,\mathrm{kg_{CO_2-eq}/kWh}$), the carbon capture efficiency of the DAC system reaches 90% and 88%, respectively. Instead, natural gas or coal as a power source reduces the carbon capture efficiency significantly: 68% and 41%, respectively. Considering wind power or solar power results in a climate change impact of $55.5\,\mathrm{g_{CO_2-eq}/MJ_{SNG}}$ and $56.4\,\mathrm{g_{CO_2-eq}/MJ_{SNG}}$, respectively. For these power sources, the climate change impact remains below the climate change impact of using fossil methane ($58.3\,\mathrm{g_{CO_2-eq}/MJ_{SNG}}$, including upstream emissions and subsequent combustion). Considering wind power, the climate change impact is composed of the impact of methane combustion (73%), electrolyzer (17%), the DAC sorbent (7%), the DAC infrastructure (2%) and the electricity supply (1%).

To evaluate the effect of different energy mixes on the environmental performance of the DAC-PtG system, the climate change and carbon capture efficiency are quantified for a range of existing energy mixes over the world (Fig-

Table 5: The environmental indicators for different power sources.

power source	electricity supply carbon footprint [kg_{CO_2-eq}/kWh]	climate change [g_{CO_2-eq}/MJ_{SNG}]	carbon capture efficiency [%]
wind	0.011	55.5	90
solar	0.044	56.4	88
natural gas	0.450	66.8	68
coal	1.000	81.0	41

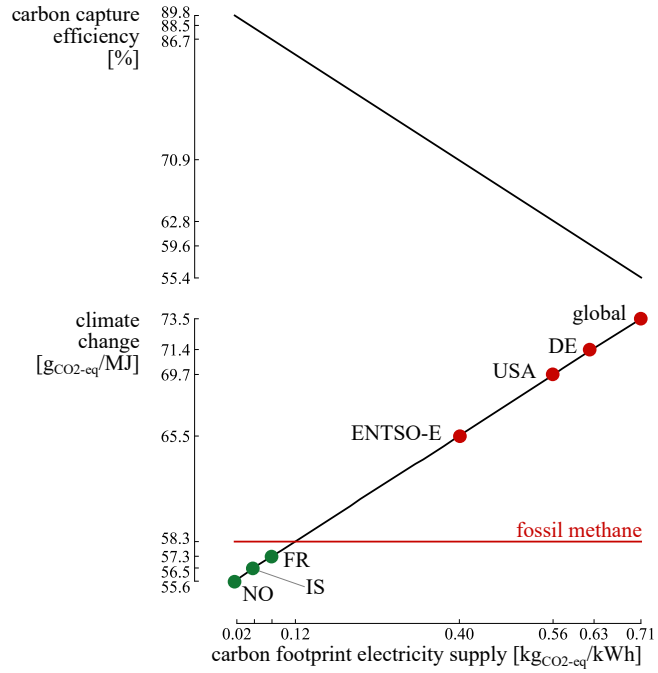

Figure 8: The environmental indicators with respect to the carbon footprint of the electricity supply indicate that an electricity supply with a carbon footprint below $0.12\,kg_{CO_2-eq}/kWh$ results in a carbon-reducing system, as the corresponding impact remains below the climate change impact of fossil methane ($58.3\,g_{CO_2-eq}/MJ_{SNG}$). This is achieved by the energy mixes of Norway (NO), Iceland (IS) and France (FR). Instead, the global energy mix and the energy mix of Germany (DE), the United States of America (USA) and the European Network of Transmission System Operators (ENTSO-E) would result in a carbon increasing system.

ure 8). An emission intensity of $0.12\,kg_{CO_2-eq}/kWh$ represents the break-even point between a system with a higher carbon footprint and a lower carbon footprint than fossil methane. These conclusions are consistent with the results of Chauvy and Dubois [41]. For the energy mixes considered, the carbon capture

efficiency situates between 55.4% (global mix) and 89.8% (Norway). For energy mixes with a carbon footprint below or equal to $0.12\,\mathrm{kg_{CO_2-eq}/kWh}$ (e.g., Norway (NO), Iceland (IS) and France (FR)), a lower impact on climate change is achieved when comparing life cycle emissions with fossil methane.

Considering the energy mix of France ($0.08\,\mathrm{kg_{CO_2-eq}/kWh}$) and the current DAC-PtG configuration, 57% of the climate change impacts are due to the production of hydrogen. At the same time, 41% are related to the DAC system and MVR unit. The results for the FD impact indicate a net reduction of about 90% for the DAC-PtG system by contrast to fossil methane, reaching $2.74\,\mathrm{g_{oil-eq}/MJ}$. Likewise, the renewable methane produced from the DAC-PtG system replaces the utilization of fossil resources such as oil and natural gas based on their energy content, and there is no fossil resource depletion in its use.

3.5. Uncertainty quantification and sensitivity analysis

The results in the previous sections are based on fixed operating parameters. However, several techno-economic parameters are uncertain and are likely to vary during the system's lifetime (Table 3). Therefore, in this section, the results on the UQ and global sensitivity analysis are provided on the exergy efficiency and the LCSNG (Subsection 3.5.1), followed by a system evaluation under varying weather conditions (Subsection 3.5.2).

3.5.1. Exergy efficiency and Levelized Cost of Synthetic Natural Gas

Considering the technical and ambient uncertainties (Table 3), a UQ on the exergy efficiency indicates that the exergy efficiency lies between 51.3% and 52.6% within 3 standard deviations. The Sobol' indices (Table 6) illustrate that the uncertainty on the exergy efficiency is mainly driven by the variability on the ambient temperature (Sobol' index of 0.36) and on the relative humidity (Sobol' index of 0.31). In addition, the uncertainty on the heat of desorption of CO_2 (Sobol' index of 0.23) and H_2O (Sobol' index of 0.20) are significant drivers of the uncertainty on the exergy efficiency as well.

Performing UQ on the LCSNG uncovers a significant uncertainty on the LCSNG, ranging between 130 €/MWh and 744 €/MWh within 3 standard deviations. The range is similar to the LCSNG reported in literature: McDonagh et al. [67] reported a price for methane between 75 €/MWh and 600 €/MWh. The uncertainty on the electricity price dominates the uncertainty on the LCSNG (Sobol' index of 0.97). In a scenario where the electricity price is fixed, the uncertainty on the DAC CAPEX (Sobol' index of 0.30), the interest rate (Sobol' index of 0.23) and the PEM electrolyzer CAPEX (Sobol' index of 0.20) drive the uncertainty on the LCSNG (Table 6). Therefore, bulk manufacturing, further maturing these technologies and more demonstration projects are required to reduce the uncertainty on the LCSNG.

3.5.2. Water content in ambient air

As highlighted in Subsection 3.1, the DAC-PtG succeeds in operating autothermally and is self-sufficient in terms of water. However, the water self-

Table 6: The Sobol' indices illustrate that the uncertainty on the ambient conditions mainly drives the uncertainty on the exergy efficiency. Instead, the uncertainty on the Levelized Cost of Synthetic Natural Gas (LCSNG) is primarily dominated by the uncertainty on the capital expenses, next to the uncertainty on the electricity price.

exergy efficiency		Levelized Cost of Synthetic Natural Gas	
parameter	Sobol' index	parameter	Sobol' index
ambient temperature	0.36	$CAPEX_{DAC}$	0.30
relative humidity	0.31	interest rate	0.23
heat desorption CO_2	0.23	$CAPEX_{PEM}$	0.20
heat desorption H_2O	0.20	inflation rate	0.07
		ambient temperature	0.07
		relative humidity	0.06
		$OPEX_{PEM}$	0.04
		$OPEX_{DAC}$	0.03

sufficiency is highly dependent on the water content in the ambient air. To illustrate how the system responds to a varying water content in the air, the relative humidity is varied in this local sensitivity analysis. Reducing the relative humidity results in a need for external water supply, i.e., $SSR_{H_2O} < 100\%$ when $\phi_{rh} < 42\%$ at an ambient temperature of 25 °C (Figure 9). However, at lower relative humidity, the water co-adsorption is lowered, which results in a lower mass flow rate in the DAC product stream. Consequently, the exergy flow to the compressors is reduced significantly (from 0.239 MW at a relative humidity of 90 % to 0.144 MW at a relative humidity of 10 %). The heat demand of the DAC unit reduces as well with a decreasing relative humidity, as less water is co-adsorbed from the air, which reduces the regeneration heat demand. Likewise, as less water is present in the DAC product stream, the exergy recuperated from cooling the product stream in the condenser decreases with decreasing relative humidity. Note that the slope of the exergetic heat recovery from both condensers in the MVR unit is steeper than the one related to the

power consumption of the compressors. This is because the sensible heat from the water and the CO_2 in the DAC product stream is also recuperated in addition to the latent heat from the water. Increasing the water vapor fraction in the DAC product stream increases the specific heat ratio of the mixture, which increases the outlet temperature of the compressor. Thus, increasing the water content in the DAC product stream increases the amount of sensible heat that can be recovered in the condenser.

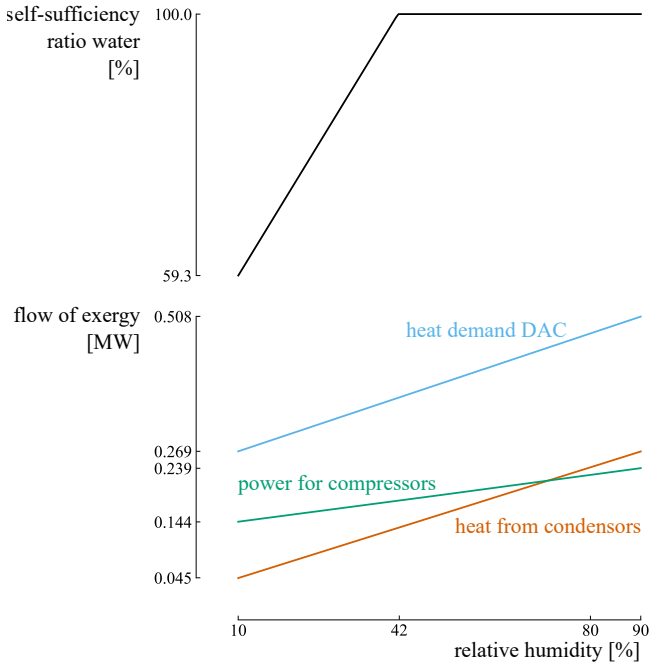

Figure 9: The evolution of the self-sufficiency ratio and flows of exergy with respect to the relative humidity illustrates that below 42 % of relative humidity, the system is not water self-sufficient. However, a reduced humidity in the ambient air reduces the power and heat demand of the compressors and Direct Air Capture (DAC) unit, respectively.

4. Conclusion

DAC is gaining interest in the concept of carbon utilization, as the economic valorization of the CO_2 into SNG provides a viable pathway to allow DAC systems to mature. Moreover, integrating low-temperature, solid sorbent DAC in PtG promises several underexplored synergies, which can lead to reducing the system energy demand.

At ambient conditions of 25 °C, 1 bar and 80% relative humidity, the DAC-PtG system operates autothermally. The two-stage MVR unit recovers 51 % of the DAC heat demand, while the remaining DAC heat (1.17 MW_{th}) is supplied by waste heat recovery from the methanation unit. In addition, under these fixed ambient conditions, the system is water self-sufficient through recycling water from the DAC product stream (1594 kg/h) and from the methanation unit (820 kg/h).

The operating conditions and the techno-economic parameters of the DAC-PtG system are still uncertain. Considering this uncertain environment, the exergy efficiency ranges between 51.3% and 52.6% within 3 standard deviations, mainly due to the uncertainty on the ambient conditions. The Levelized Cost of Synthetic Natural Gas (LCSNG) ranges between 130 €/MWh and 744 €/MWh within 3 standard deviations, mainly driven by an uncertain electricity price. On a component level, the uncertainty on the expenses related to DAC and electrolysis are the main drivers. Therefore, bulk manufacturing, further maturing these technologies and more demonstration projects are required to reduce the uncertainty on the LCSNG. The DAC-PtG has a lower carbon footprint than fossil

methane when the carbon footprint of the electricity supply is below or equal to $0.12\,\mathrm{kg_{CO_2-eq}/kWh}$. Using only wind turbines or photovoltaic panels to power the DAC-PtG system results in a carbon capture efficiency of 90 % and 88 %, respectively. For such power systems, the DAC-PtG system achieves a climate change impact ($55.5\,\mathrm{g_{CO_2-eq}/MJ_{SNG}}$ and $56.4\,\mathrm{g_{CO_2-eq}/MJ_{SNG}}$, respectively) below the climate change impact of fossil methane ($58.3\,\mathrm{g_{CO_2-eq}/MJ_{SNG}}$).

In future work, we will add energy storage and intermittent renewable energy sources, i.e., photovoltaic panels and wind turbines, and corresponding time series on the solar irradiance, wind speed, ambient temperature and humidity. In addition, we will perform a design optimization on the storage size and DAC-PtG operating conditions to ensure an optimized and stable operation under varying ambient conditions.

5. Acknowledgements

The authors express their gratitude to the SPF Economie (Belgium) for funding the DRIVER project in the framework of the Energy Transition Fund program. Diederik Coppitters acknowledges the support of the Fonds de la Recherche Scientifique - FNRS [CR 40011127]. Remi Chauvy also thanks the support from the *NCKU 90 and Beyond* Initiative, as well as Taiwan's Ministry of Education (MOE) for subsidizing the Program on Bilingual Education for Students in College, in National Cheng Kung University (NCKU) Bilingual Education Research Center.

References

[1] D. Coppitters, W. De Paepe, F. Contino, Robust design optimization of a photovoltaic-battery-heat pump system with thermal storage under aleatory and epistemic uncertainty, Energy (2021) 120692.

[2] P. Huang, M. Lovati, X. Zhang, C. Bales, S. Hallbeck, A. Becker, H. Bergqvist, J. Hedberg, L. Maturi, Transforming a residential building cluster into electricity prosumers in Sweden: Optimal design of a coupled PV-heat pump-thermal storage-electric vehicle system, Applied Energy 255 (2019) 113864.

[3] D. Coppitters, K. Verleysen, W. De Paepe, F. Contino, How can renewable hydrogen compete with diesel in public transport? Robust design optimization of a hydrogen refueling station under techno-economic and environmental uncertainty, Applied Energy 312 (2022) 118694.

[4] R. Batten, O. Galant, M. Karanjikar, S. Spatari, Meeting sustainable aviation fuel policy targets through first generation corn biorefineries, Fuel 333 (2023) 126294.

[5] M. Wei, C. A. McMillan, et al., Electrification of industry: potential, challenges and outlook, Current Sustainable/Renewable Energy Reports 6 (4) (2019) 140–148.

[6] X. Rixhon, G. Limpens, D. Coppitters, H. Jeanmart, F. Contino, The Role of Electrofuels under Uncertainties for the Belgian Energy Transition, Energies 14 (13) (2021) 4027.

[7] D. Coppitters, W. De Paepe, F. Contino, Surrogate-assisted robust design optimization and global sensitivity analysis of a directly coupled photovoltaic-electrolyzer system under techno-economic uncertainty, Applied Energy 248 (2019) 310–320.

[8] M. Aziz, Liquid hydrogen: A review on liquefaction, storage, transportation, and safety, Energies 14 (18) (2021) 5917.

[9] M. Qi, Y. Liu, T. He, L. Yin, C.-M. Shu, I. Moon, System perspective on cleaner technologies for renewable methane production and utilisation towards carbon neutrality: Principles, techno-economics, and carbon footprints, Fuel 327 (2022) 125130.

[10] E. Billig, D. Thraen, Renewable methane–a technology evaluation by multi-criteria decision making from a european perspective, Energy 139 (2017) 468–484.

[11] A. C. Ince, C. O. Colpan, A. Keles, M. F. Serincan, U. Pasaogullari, Scaling and performance assessment of power-to-methane system based on an operation scenario, Fuel 332 (2023) 126182.

[12] G. Reiter, J. Lindorfer, Evaluating CO2 sources for power-to-gas applications–A case study for Austria, Journal of CO2 Utilization 10 (2015) 40–49.

[13] S. Budinis, Direct air capture, Tech. rep., International Energy Agency (2021).

[14] C. Pritchard, A. Yang, P. Holmes, M. Wilkinson, Thermodynamics, economics and systems thinking: what role for air capture of CO2?, Process Safety and Environmental Protection 94 (2015) 188–195.

[15] A. Goeppert, M. Czaun, G. S. Prakash, G. A. Olah, Air as the renewable carbon source of the future: an overview of CO2 capture from the atmosphere, Energy & Environmental Science 5 (7) (2012) 7833–7853.

[16] X. Wu, R. Krishnamoorti, P. Bollini, Technological Options for Direct Air Capture: A Comparative Process Engineering Review, Annual Review of Chemical and Biomolecular Engineering 13 (2022).

[17] M. Fasihi, O. Efimova, C. Breyer, Techno-economic assessment of CO2 direct air capture plants, Journal of cleaner production 224 (2019) 957–980.

[18] N. McQueen, K. V. Gomes, C. McCormick, K. Blumanthal, M. Pisciotta, J. Wilcox, A review of direct air capture (DAC): scaling up commercial technologies and innovating for the future, Progress in Energy 3 (3) (2021) 032001.

[19] C. Tregambi, P. Bareschino, D. P. Hanak, F. Montagnaro, F. Pepe, E. Mancusi, Modelling of an integrated process for atmospheric carbon dioxide capture and methanation, Journal of Cleaner Production 356 (2022) 131827.

[20] E. S. Sanz-Pérez, C. R. Murdock, S. A. Didas, C. W. Jones, Direct capture of CO2 from ambient air, Chemical reviews 116 (19) (2016) 11840–11876.

[21] J. V. Veselovskaya, P. D. Parunin, O. V. Netskina, A. G. Okunev, A novel process for renewable methane production: combining direct air capture by K_2CO_3/alumina sorbent with CO_2 methanation over Ru/alumina catalyst, Topics in Catalysis 61 (2018) 1528–1536.

[22] C. Jeong-Potter, R. Farrauto, Feasibility study of combining direct air capture of CO2 and methanation at isothermal conditions with dual function materials, Applied Catalysis B: Environmental 282 (2021) 119416.

[23] C. Jeong-Potter, M. Abdallah, C. Sanderson, M. Goldman, R. Gupta, R. Farrauto, Dual function materials (Ru+ Na2O/Al2O3) for direct air capture of CO2 and in situ catalytic methanation: The impact of realistic ambient conditions, Applied Catalysis B: Environmental 307 (2022) 120990.

[24] C. Drechsler, D. W. Agar, Intensified integrated direct air capture-power-to-gas process based on H2O and CO2 from ambient air, Applied Energy 273 (2020) 115076.

[25] C. Drechsler, D. W. Agar, Investigation of water co-adsorption on the energy balance of solid sorbent based direct air capture processes, Energy 192 (2020) 116587.

[26] M. Berger, D. Radu, G. Detienne, T. Deschuyteneer, A. Richel, D. Ernst, Remote Renewable Hubs for Carbon-Neutral Synthetic Fuel Production, Frontiers in Energy Research (2021) 200.

[27] U. Caldera, C. Breyer, Learning curve for seawater reverse osmosis desalination plants: capital cost trend of the past, present, and future, Water Resources Research 53 (12) (2017) 10523–10538.

[28] U. Caldera, D. Bogdanov, C. Breyer, Local cost of seawater RO desalination based on solar PV and wind energy: A global estimate, Desalination 385 (2016) 207–216.

[29] P. Talebizadehsardari, M. Ehyaei, A. Ahmadi, D. Jamali, R. Shirmohammadi, A. Eyvazian, A. Ghasemi, M. A. Rosen, Energy, exergy, economic, exergoeconomic, and exergoenvironmental (5E) analyses of a triple cycle with carbon capture, Journal of CO2 Utilization 41 (2020) 101258.

[30] N. Norouzi, M. Hosseinpour, S. Talebi, M. Fani, A 4E analysis of renewable formic acid synthesis from the electrochemical reduction of carbon dioxide and water: studying impacts of the anolyte material on the performance of the process, Journal of Cleaner Production 293 (2021) 126149.

[31] Z. Tian, Z. Qi, W. Gan, M. Tian, W. Gao, A novel negative carbon-emission, cooling, and power generation system based on combined LNG regasification and waste heat recovery: Energy, exergy, economic, environmental (4E) evaluations, Energy (2022) 124528.

[32] C. Drechsler, D. W. Agar, Characteristics of DAC operation within integrated PtG concepts, International Journal of Greenhouse Gas Control 105 (2021) 103230.

[33] National Research Council, Climate Intervention: Carbon Dioxide Removal and Reliable Sequestration, National Academies Press, 2015.

[34] I. H. Bell, J. Wronski, S. Quoilin, V. Lemort, Pure and pseudo-pure fluid thermophysical property evaluation and the open-source thermophysical property library CoolProp, Industrial & engineering chemistry research 53 (6) (2014) 2498–2508.

[35] D. Coppitters, W. De Paepe, F. Contino, Robust design optimization and stochastic performance analysis of a grid-connected photovoltaic system with battery storage and hydrogen storage, Energy 213 (2020) 118798.

[36] A. Buttler, H. Spliethoff, Current status of water electrolysis for energy storage, grid balancing and sector coupling via power-to-gas and power-to-liquids: A review, Renewable and Sustainable Energy Reviews 82 (2018) 2440–2454.

[37] Z. Abdin, C. J. Webb, E. M. Gray, Modelling and simulation of a proton exchange membrane (PEM) electrolyser cell, International Journal of Hydrogen Energy 40 (39) (2015) 13243–13257.

[38] F. Marangio, M. Santarelli, M. Calì, Theoretical model and experimental analysis of a high pressure PEM water electrolyser for hydrogen production, International Journal of Hydrogen Energy 34 (3) (2009) 1143–1158.

[39] R. García-Valverde, N. Espinosa, A. Urbina, Simple PEM water electrolyser model and experimental validation, International Journal of Hydrogen Energy 37 (2) (2012) 1927–1938.

[40] M. Mori, T. Mržljak, B. Drobnič, M. Sekavčnik, Integral characteristics of hydrogen production in alkaline electrolysers, Strojniški vestnik-Journal of Mechanical Engineering 59 (10) (2013) 585–594.

[41] R. Chauvy, L. Dubois, Life cycle and techno-economic assessments of direct air capture processes: An integrated review, International Journal of Energy Research (2022).

[42] W. Brilman, CO2 removal from air, in: Advances in Carbon Capture, Elsevier, 2020, pp. 523–543.

[43] R. Veneman, Adsorptive systems for post-combustion co2 capture: design, experimental validation and evaluation of a supported amine based process, Ph.D. thesis, UTwente (2015).

[44] R. Veneman, N. Frigka, W. Zhao, Z. Li, S. Kersten, W. Brilman, Adsorption of H2O and CO2 on supported amine sorbents, International journal of greenhouse gas control 41 (2015) 268–275.

[45] K. S. Lackner, S. Brennan, J. M. Matter, A.-H. A. Park, A. Wright, B. Van Der Zwaan, The urgency of the development of CO2 capture from ambient air, Proceedings of the National Academy of Sciences 109 (33) (2012) 13156–13162.

[46] A. Lewandowska-Bernat, U. Desideri, Opportunities of power-to-gas technology in different energy systems architectures, Applied energy 228 (2018) 57–67.

[47] R. Chauvy, D. Verdonck, L. Dubois, D. Thomas, G. De Weireld, Techno-economic feasibility and sustainability of an integrated carbon capture and conversion process to synthetic natural gas, Journal of CO2 Utilization 47 (2021) 101488.

[48] R. Chauvy, L. Dubois, P. Lybaert, D. Thomas, G. De Weireld, Production of synthetic natural gas from industrial carbon dioxide, Applied Energy 260 (2020) 114249.

[49] T. J. Kotas, The exergy method of thermal plant analysis, Paragon Publishing, 2012.

[50] A. D. McNaught, A. Wilkinson, et al., Compendium of chemical terminology, Vol. 1669, Blackwell Science Oxford, 1997.

[51] B. Zakeri, S. Syri, Electrical energy storage systems: A comparative life cycle cost analysis, Renewable and sustainable energy reviews 42 (2015) 569–596.

[52] S. Niaz, T. Manzoor, A. H. Pandith, Hydrogen storage: Materials, methods and perspectives, Renewable and Sustainable Energy Reviews 50 (2015) 457–469.

[53] Triami Media BV, Historic inflation Belgium - CPI inflation, Available online: `inflation.eu/inflation-rates/belgium/historic-inflation/cpi-inflation-belgium.aspx`. Accessed: 1st August 2020 (2019).

[54] S. Deutz, A. Bardow, Life-cycle assessment of an industrial direct air cap-

ture process based on temperature–vacuum swing adsorption, Nature Energy 6 (2) (2021) 203–213.

[55] K. Madhu, S. Pauliuk, S. Dhathri, F. Creutzig, Understanding environmental trade-offs and resource demand of direct air capture technologies through comparative life-cycle assessment, Nature Energy 6 (11) (2021) 1035–1044.

[56] R. Chauvy, L. Dubois, D. Thomas, G. De Weireld, Environmental impacts of the production of synthetic natural gas from industrial carbon dioxide, Sustainable Production and Consumption 30 (2022) 301–315.

[57] K. Bareiß, C. de la Rua, M. Möckl, T. Hamacher, Life cycle assessment of hydrogen from proton exchange membrane water electrolysis in future energy systems, Applied Energy 237 (2019) 862–872.

[58] G. Mavromatidis, K. Orehounig, J. Carmeliet, A review of uncertainty characterisation approaches for the optimal design of distributed energy systems, Renewable and Sustainable Energy Reviews 88 (2018) 258–277.

[59] S. Van Erdeweghe, J. Van Bael, W. D'haeseleer, Costing methods for combined heat-and-power plants fueled by zero-marginal cost energy sources, Energy Conversion and Management 187 (2019) 122–132.

[60] C. Navas, Development of Business Cases for Fuel Cells and Hydrogen Applications for Regions and Cities - FCH Heavy-duty trucks, Fuel Cells and Hydrogen 2 Joint Undertaking (2017).

[61] J. Gorre, F. Ruoss, H. Karjunen, J. Schaffert, T. Tynjälä, Cost benefits of optimizing hydrogen storage and methanation capacities for Power-to-Gas plants in dynamic operation, Applied Energy 257 (2020) 113967.

[62] D. Coppitters, P. Tsirikoglou, W. De Paepe, K. Kyprianidis, A. Kalfas, F. Contino, RHEIA: Robust design optimization of renewable Hydrogen and dErIved energy cArrier systems, Journal of Open Source Software 7 (75) (2022) 4370.

[63] B. Sudret, Polynomial chaos expansions and stochastic finite-element methods, Risk and Reliability in Geotechnical Engineering Chap. 6 (2003) (2014) 265–300.

[64] M. Ozkan, S. P. Nayak, A. D. Ruiz, W. Jiang, Current status and pillars of direct air capture technologies, Iscience (2022) 103990.

[65] M. A. Rosen, I. Dincer, A study of industrial steam process heating through exergy analysis, International journal of energy research 28 (10) (2004) 917–930.

[66] D. Burrin, S. Roy, A. P. Roskilly, A. Smallbone, A combined heat and green hydrogen (CHH) generator integrated with a heat network, Energy Conversion and Management 246 (2021) 114686.

[67] S. McDonagh, R. O'Shea, D. M. Wall, J. P. Deane, J. D. Murphy, Modelling of a power-to-gas system to predict the levelised cost of energy of an advanced renewable gaseous transport fuel, Applied Energy 215 (2018) 444–456.